REPORT DOCUMENTATION PAGE

Form Approved
OMB No. 0704-0188

1. AGENCY USE ONLY *(LEAVE BLANK)*	2. REPORT DATE	3. REPORT TYPE AND DATES COVERED
	22 April 1999	Professional Paper

4. TITLE AND SUBTITLE

Experimental Investigation of Vortex-Tail Interaction on a 76/40 Degree Double-Delta Wing

5. FUNDING NUMBERS

6. AUTHOR(S)

Terence A. Ghee Hugo A. Gonzalez David B. Findlay

7. PERFORMING ORGANIZATION NAME(S) AND ADDRESS(ES)

Naval Air Warfare Center Aircraft Division
22347 Cedar Point Road, Unit #6
Patuxent River, Maryland 20670-1161

8. PERFORMING ORGANIZATION REPORT NUMBER

9. SPONSORING/MONITORING AGENCY NAME(S) AND ADDRESS(ES)

Naval Air Systems Command
47123 Buse Road, Unit IPT
Patuxent River, Maryland 20670-1547

10. SPONSORING/MONITORING AGENCY REPORT NUMBER

11. SUPPLEMENTARY NOTES

12a. DISTRIBUTION/AVAILABILITY STATEMENT

Approved for public release; distribution is unlimited.

12b. DISTRIBUTION CODE

13. ABSTRACT *(Maximum 200 words)*

An experimental investigation was conducted to quantify the vortex-tail interaction on a 76/40 degree double-delta wing model. The effects of different fillets at the wing/strake juncture, tail span-wise positions, and angles-of-attack were evaluated. The vertical tails were instrumented with 28 fast-response pressure transducers. Pressure time histories and frequency power spectral densities were analyzed for 35 configurations. Angle-of-attack was varied from -2 to 40 degrees, tunnel dynamic pressure was 26.74 psf and Reynolds number was 1.3 million. The results show a strong dependence on fillet geometry, tail position, transducer measurement location, and angle-of-attack on the magnitude and frequency of the tail response to the vortex forcing. In addition, a low frequency pulse was found that contained tremendous energy.

14. SUBJECT TERMS

Double-delta Vortex-tail

15. NUMBER OF PAGES

18

16. PRICE CODE

17. SECURITY CLASSIFICATION OF REPORT	18. SECURITY CLASSIFICATION OF THIS PAGE	19. SECURITY CLASSIFICATION OF ABSTRACT	20. LIMITATION OF ABSTRACT
Unclassified	Unclassified	Unclassified	UL

EXPERIMENTAL INVESTIGATION OF VORTEX-TAIL INTERACTION ON A 76/40 DEGREE DOUBLE-DELTA WING

Terence A. Ghee*, Hugo A. Gonzalez†, and David B. Findlay‡
Naval Air Systems Command
Patuxent River, MD 20670 USA

ABSTRACT

An experimental investigation was conducted to quantify the vortex-tail interaction on a 76/40 degree double-delta wing model. The effects of different fillets at the wing/strake juncture, tail span-wise positions, and angles-of-attack were evaluated. The vertical tails were instrumented with twenty-eight fast-response pressure transducers. Pressure time histories and frequency power spectral densities were analyzed for thirty-five configurations. Angle-of-attack was varied from -2 to 40 degrees, tunnel dynamic pressure was 26.74 psf and Reynolds number was 1.3 million. The results show a strong dependence on fillet geometry, tail position, transducer measurement location, and angle-of-attack on the magnitude and frequency of the tail response to the vortex forcing. In addition, a low frequency pulse was found that contained tremendous energy.

NOMENCLATURE

a_∞	speed of sound, 1155 ft/s
A	constant, b/ V_∞, 0.0091 /sec
AR	aspect ratio, 2.41
b	span, 1.36 ft
c	chord, ft
c_R	root chord, 1.33ft
c_{Rtail}	tail root chord, 0.38 ft
c_t	tip chord, 0.21 ft
c_{ttail}	tail tip chord, 0.13 ft
C	coherence
C_p	pressure coefficient, $p-p_\infty/q_\infty$
f	frequency, Hz
G	amplifier gain
I_{raw}	raw integer value (digital)
M_∞	freestream Mach number, V_∞/ a_∞, 0.13
P	pressure, psi
P_{Ref}	reference pressure, psi
PSD	power spectral density
q_∞	tunnel dynamic pressure, 26.74 psf
Re	Reynolds number, $(\rho_\infty V_\infty C_R)/\mu_\infty$, 1.3E6
RMS	root mean square
std	standard deviation
Se	transducer sensitivity, volt/psi
S	wing area, 0.768 ft^2
S_{tail}	tail area, 0.093 ft^2
St	Strouhal number, (b f)/ V_∞
t	time, sec
t_{max}	model maximum thickness, 0.0313 ft
V	excitation voltage, 10 volt
V_∞	tunnel freestream velocity, 150 ft/s
α	geometric angle of attack, degree
λ	taper ratio, 0.16
λ_{tail}	tail taper ratio, 0.33
μ_∞	viscosity, 3.7373E-7, slug/(ft sec)
τ	non-dimensional time, $(t\ a_\infty)/c_R$

INTRODUCTION

Modern fighter/attack air vehicles rely on vortex lift to allow the vehicle to achieve high angle-of-attack flight. Typically, a leading edge extension (LEX) is combined with a modified delta wing. The LEX surface creates a pair of vortices that generate significant lift. However, the use of vortex lift is not without a downside. Impingement of the burst LEX vortices on the vertical tail of a modern fighter/attack air vehicle was found to cause fatigue and premature replacement of the vertical tails. It is thought that the breakdown of the LEX vortex impinged upon the vertical tails at a frequency close to a structural vibratory mode. Many researchers in recent years have focused on quantifying the effect of the LEX vortex on vertical tails.[1-4]

As part of a continuing effort, a wind tunnel test was conducted using a 76/40 degree double delta wing with instrumented vertical tails. Unique to this experiment, the model included a variety of wing/strake juncture fillet shapes. In addition, the vertical tails were able to be moved spanwise and streamwise (the present investigation constrained the tails streamwise in the most forward position). Pressure time histories were

* Aerodynamicist, Senior Member AIAA
† Aerodynamicist, Senior Member AIAA
‡ Aero Technology Team Lead, Member AIAA

recorded and analyzed in the time and frequency domains to quantify the response sensed on the vertical tails to the vortex forcing.

EXPERIMENTAL APPARATUS

The tests were conducted in the Naval Aerodynamic Test Facility (NATF). The NATF is a four-foot by four-foot closed test section, open-return wind tunnel. The facility incorporates a 200 horsepower motor that drives a variable pitch fan and delivers a maximum velocity of 205 ft/s. In addition, the facility has honeycomb and three sets of flow conditioning screens. Fig. 1 shows the 76/40 degree double-delta wing in the NATF.

The model used in the present investigation consisted of a 76/40 degree double-delta wing with vertical tails mounted on booms aft of the wing. Manufactured of stainless steel, the model featured a flat upper surface with sharp, 20 degree beveled edges, see Fig. 2.

Four sets of fillets, shown in Fig. 3, were used in the present investigation: a baseline (no fillet, F1), linear (F2), diamond (F3), and parabolic (F4). Each fillet planform area was 1% of total wing planform area. Thus, starboard and port fillets combined to total 2% of the wing planform area. Details of the fillet geometry, design, and effect on aerodynamic performance may be found in Refs. 5 and 6.

The rigid vertical tails were attached to booms that were then mounted to the underside of the wing. The booms could be positioned in four spanwise locations, see Fig. 4. The tails were instrumented with 28 Kulite fast-response, differential-gage pressure transducers: the starboard tail had twelve transducers on the inboard and outboard side, see Fig. 5. The port tail had transducers located equivalent to transducers 9, 10, 13, and 14 on the starboard tail. These port tail transducer locations proved unfortunate as the strongest response was seen along the leading edge of the vertical tails. The tails were positioned normal to the wing surface and had an 18.43 degree leading and trailing edge sweep angle. A cover plate spanned the area between the tails.

A short sting assembly attached to the facility pitch strut supported the model. Due to an error in mounting the support system turntable, a -1.344 degree sideslip angle was introduced. In recent tests in the NATF, the cross-flow angle was determined to be -0.09 degrees. Thus, the error in sideslip was –1.254 degrees. Also, the support system was constrained vertically; the model moved off-centerline with changing angle-of-attack.

The data were acquired using a Sheldon SI-100 16-bit, 32-input data-acquisition system connected to a personal computer. This system sampled the data in a muliplex fashion. Thus, data coincidence was not possible with this system.

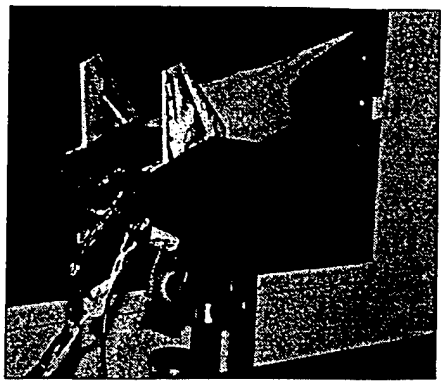

Figure 1 - 76/40 degree double-delta wing model in NATF

PROCEDURE AND DATA REDUCTION

The tests were conducted at a constant tunnel velocity of 150 ft/s (q_∞=26.74 ft/s and Reynolds number of 1.3 million based on root chord). Reynolds number sweeps were performed but have not been reduced at the present time. Washburn, *et. al*[1] showed little effect of Reynolds number on the buffet response. This is not surprising as the flowfield is dominated by a vortex system emanating from a sharp leading edge. Model incidence was varied from -2 degrees to 40 degrees. More specifically: -2, 0, 2, 10, 16, 18, 20, 22, 24, 26, 28, 30, 32, 36, and 40 degrees. Five seconds of wind-off-zero data were acquired previous to tunnel start up. The transducers were then nulled and the tunnel was driven to 150 ft/s. After test conditions steadied, unsteady pressure data was acquired. Unsteady tail pressures were sampled at 8,192 samples/second for 30 seconds. A Bessel filter provided a low-pass cut off frequency of 2,212 Hz. Following tunnel shutdown, wind-off-zero data were acquired for comparison to the pre-test wind-off-zero data. The tails were tested at the most forward location on the booms at three spanwise locations (T1, T2, and T4 in Fig. 4) for each fillet and the baseline configuration.

The data was first analyzed to cull the vast amount of data to a workable amount. A custom Labview software routine was used to look at all the data and choose those configurations where significant tail-vortex interactions occurred. In this manner, approximately 120 configurations were perused and reduced to 35 configurations to be analyzed. For each of the 35 configurations, all 28 transducers were evaluated to determine the time history and PSD characteristics.

The large size of the data array (245,760 samples

per transducer per run) necessitated the data be

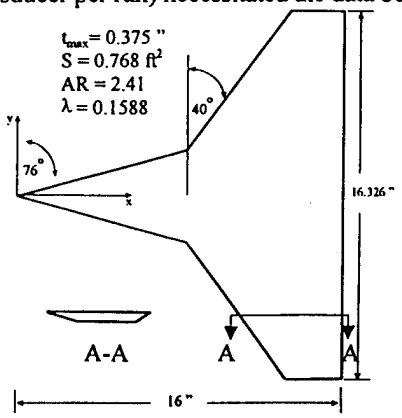

Figure 2 - Schematic of 76/40 degree double-delta wing

analyzed on a high performance computer system. Matlab software was used to determine the pressure time history and pressure power spectral density (PSD) using an SGI Power Challenge Array located at the Army Research Laboratory (ARL).

The data was converted to engineering units using the following:

$$P - P_{Ref} = \frac{[(I_{raw} * V)/65{,}535]}{G*Se} \qquad (psi)$$

The assumption was made that the wind-off-zero pressure was essentially total pressure. At the time of the test, a barometric pressure device was not available. Thus, tunnel static pressure was determined by subtracting the tunnel dynamic pressure from the wind-off-zero (or total) pressure. Pressure coefficient data were determined by the following:

$$C_P = \frac{[(P_{measured} - P_{Ref}) - (P_{wind\text{-}off\ zero} - P_{Ref})] - (q_\infty/144)}{(q_\infty/144)}$$

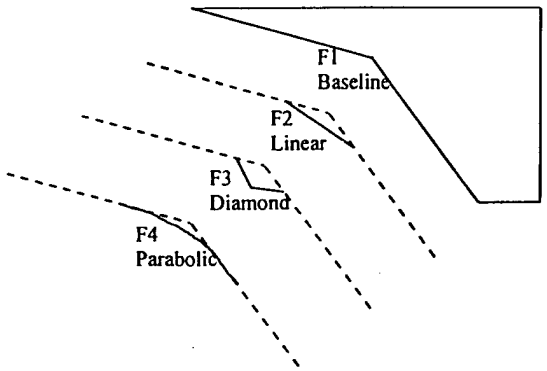

Figure 3 - Fillet geometry

The coherent acoustic noise present in the freestream data was removed from the tail pressure measurements by assuming the model oriented at zero degrees incidence measured freestream noise. The coherence was a function of the power spectrum of the freestream noise (determined when the model was at zero incidence) and the power spectrum of the data at an arbitrary angle-of-attack and the cross spectrum of the freestream noise and the data at the arbitrary angle-of-attack, see Ref. 1 and 7. Thus, the coherence was found by:

$$C = \frac{(PSD_{zero,\ meas})^2}{(PSD_{zero,\ zero})^* (PSD_{meas,\ meas})}$$

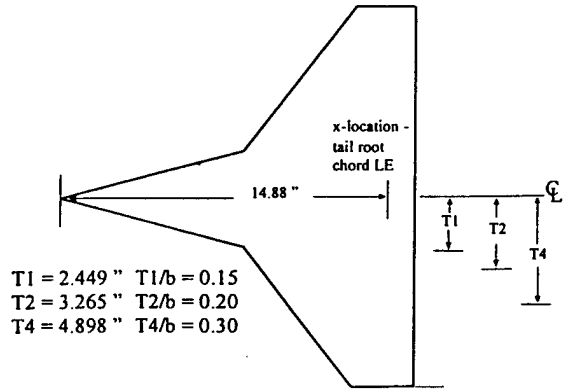

Figure 4 - Vertical tail location

The PSD of the measured data is then:

$$PSD_{meas} = (1 - C) * PSD_{meas,\ uncorrected} \qquad (RMS^2)$$

The algorithm to determine the PSD was based on the method by Welch[8]. The data were segmented into windows to allow thirty averages and corresponded to a frequency resolution of 1 Hz. No data overlapping was employed and a Hanning filter was used with a window length the same size as the data segments. The mean was eliminated from the PSD and coherence calculations and a 95% confidence criteria was used to gage the PSD assessment.

A weighting factor was introduced to the PSD amplitude following a convention prescribed by Mabey[9]:

$$(St * PSD)^{0.5} \text{ or } (A * f * PSD)^{0.5}$$

Thus, the amplitude of the PSD is weighted by multiplying the incremental frequency to the corresponding PSD amplitude. This method reduced PSD amplitudes occurring at low frequencies.

RESULTS

Buffet Standard Deviation

The pressure time histories were analyzed to determine the standard deviation from the mean as a gage of the relative strength of the tail buffet. Note, the notation F#T# is used to describe the fillet shape and tail position. For example, F1T2, is the baseline fillet with the tails in position 2 (see Figs. 3 and 4 for the other fillet and tail notations).

As shown in Figs. 6 through 9, tail pressure buffet response standard deviation, in coefficient form, is plotted versus angle-of-attack for transducers along the leading edge of the starboard tail. Maximum standard deviation from the mean pressure generally occurred at the inboard root leading edge. In fact, quite often the pressures calculated for the other transducer locations were quite insignificant by comparison. Therefore, the port tail transducers, which were located along the tail centerline proved to sense rather low levels of tail buffet.

In general, maximum buffet pressure response occurred on the inboard side of the tail leading edge for the various fillet shapes tested. The outboard leading edge pressure transducer locations were seen to have buffet peaks at angles-of-attack significantly lower than the inboard leading edge pressure transducer locations (16 to 22 degrees for the outboard locations as opposed to 32 to 36 degrees for the inboard transducers, c.f. Fig. 9).

Fig. 10 compares the effect of fillet shapes on tail buffet pressure response at the inboard root leading edge (Transducer 1) for different tail positions. The parabolic fillet was seen to generate the maximum tail buffet, followed by the linear fillet. The diamond fillet was seen to generate the least amount of tail buffet. In addition to the reduced tail buffet pressure signature of the diamond fillet, Ref. 5 reported the use of diamond fillets (as well as the other fillets) to significantly increase the maximum lift coefficient by 18%. The diamond fillet may also have the advantage of reduced low observable (LO) characteristics.

As seen in Fig. 10c, the parabolic fillet exhibited substantially more tail buffet for the tails positioned farthest outboard. It is due to the manner that the vortex is formed that explains this difference. Refs. 5 and 6 presented CFD streamlines of the flow over the wing. It was found that the strake vortex smoothly combined with the wing vortex into essentially one large vortex system. This parabolic fillet vortex system appeared to be more outboard of the vortices generated by the other fillets. Also, because there were no wing/strake leading edge discontinuities, the vortex system was stronger. The diamond fillet, by comparison, creates a number of vortices from each leading edge discontinuity. Thus, it is not surprising that the parabolic fillet provides the strongest tail buffet pressure response and the diamond fillet provides the weakest tail buffet pressure response.

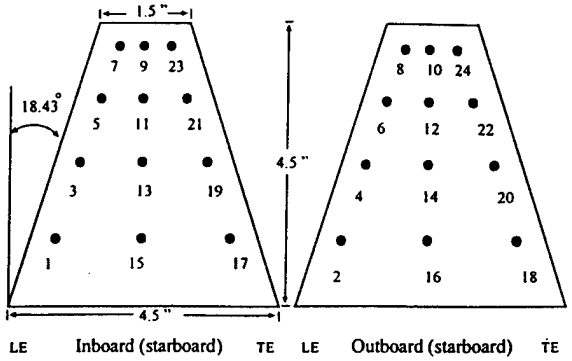

Figure 5 - Transducer location on vertical tails

The effect of tail position on buffet pressure response, for a given fillet, failed to provide a consistent pattern, see Fig. 11. In general, for a given fillet, the curves exhibited the same general shape.

PSD and Time history plots

Table 1 summarizes the location of the maximum weighted PSD amplitude, $(St * PSD)^{0.5}$, and corresponding frequency for a given configuration. That is, for a given configuration (angle-of-attack, fillet shape, etc.) all transducers were analyzed to find a single maximum weighted value for PSD amplitude and corresponding frequency. Amplitude data annotated with a (C) in Table 1 indicate that the data were clipped.

Analysis of the location of the maximum peak of weighted PSD amplitude frequencies was shown to occur along the leading edge of the vertical tails. A majority of the frequencies were shown to occur at the inboard root leading edge (Transducer 1). Further, analysis showed that the frequency of the maximum amplitude varied with fillet shape, tail location, transducer location, and angle-of-attack. Significant amplitude values existed on the tail at frequencies different than those reported in Table 1. For example, it was noted that the frequencies along the tail tip were often different from the frequency measured along the root leading edge. The frequency also varied inboard versus outboard. Therefore, quantifying the frequency of the buffet pressure response does not easily lend itself to a single value.

As noted in the previous section, the parabolic fillet was seen to produce the greatest amount of tail buffet and the diamond was seen to experience the least amount of tail buffet. This trend is born out in Fig. 12 by viewing the peak weighted PSD amplitude for each configuration. The data presented in Fig. 12 is located on the starboard tail, inboard root leading edge (Transducer 1) for an angle-of-attack of 32 degrees and

tail position 2 and is representative of the frequency domain data base. In addition to the diminished amplitude of the diamond fillet configuration, the characteristic frequency was seen to be higher than the baseline configuration characteristic frequency. Such a frequency increase could be beneficial by shifting the characteristic frequency of the vortex system away from the natural frequency of the tails. Thus, buffet alleviation can occur by reducing the amplitude or moving the characteristic frequency of the vortex system away from the tail natural frequency.

The corresponding non-dimensional time history plots for this configuration are presented in Fig. 13 and represents one second of data. The diamond fillet was seen to have the lowest values of peak-to-peak amplitude while the parabolic fillet had the greatest peak-to-peak amplitude.

Figs. 14 and 15 show the effect of varying tail position on tail buffet response (frequency and time domain) at the root, inboard, leading edge (Transducer 1) for a baseline fillet at 32 degrees angle-of-attack. Peak frequency was seen to vary with tail location and have the lowest value at tail position two (T2). Maximum amplitude for all tail positions was essentially the same.

Figs. 16 and 17 show the response (frequency and time domain) at the root, inboard, leading edge (Transducer 1) for a parabolic fillet at 32 degrees angle-of-attack. A double frequency peak is seen at the most inboard tail position, see Fig. 16a. Ref. 1 reported a similar double peak phenomenon but on a 76 degree delta wing. Viewing Fig. 16, it would appear a trend of decreasing peak frequency with increasing spanwise tail location. However, in Table 1, the maximum frequency was found to occur for the most inboard tail location (T1) at Transducer 8 (leading edge, tip, outboard) and at the frequency of the first frequency peak in Fig. 16a.

Figs. 18 and 19 show the difference in a buffet response inboard versus outboard at the root leading edge for a parabolic fillet for tail location 2 at 32 degrees angle-of-attack. The inboard transducer recorded a higher buffet value, perhaps as a result of the rotation of the vortex system. It may also be influenced by vortices associated with the vertical tail itself. In Fig. 18, the peak frequencies correspond well inboard versus outboard. However, this trend was not always followed.

During the course of data analysis, a number of significant pulses for the configurations F2T1, F4T1, and F4T4 were seen to occur at very low frequency (under 1 Hz). A typical example is shown in Figs. 20 and 21. The pulses seen in Fig. 21a were on the order of 0.3 Hz and sometimes contained a tremendous amount of energy, see Figs. 22 and 23. At present, the cause of this phenomenon is undetermined. Based on results of Refs. 10 - 12, a potential cause may be the movement of the vortex breakdown location. Fig. 22b shows the tremendous amount of buffet energy impinging on the tails at low frequency. The units of the y-axis of Figs. 20b and 22b are not the same as the units of the y-axis of Figs. 20a and 22a. That is, the amplitude in Figs. 20b and 22b has been "de-weighted" and just the PSD amplitude has been depicted.

If one counts the number of pulses seen in the time history (Fig. 23a), this approximates the frequency of the large spike seen in Fig. 22b. Fig. 23a also exhibits evidence of transducer clipping. Clipping was seen in some isolated configurations but was thought not to be the cause of the tremendous low frequency pulse seen in Fig. 22b because there were a number of other cases that did not exhibit clipping but yet still contained a similar high-strength, low-frequency pulse. The pulses were seen at a number of locations along the tail leading edge, outboard and inboard, and were more pronounced at locations closer to the tail tip. It should be noted that these very large amplitude, low frequency buffet pulses have as yet only been found for the linear and parabolic fillet. The low frequency pulse has been recently repeated in a follow-on test. The follow-on test included the effects of canted tail angles and utilized on- and off-body flow visualization.

CONCLUSIONS

A test was conducted to determine the effect of LEX vortex buffet response on a set of pressure instrumented tails mounted on a 76/40 degree double delta wing model. Spanwise tail position, angle-of-attack, and LEX/wing juncture fillet shape were varied parametrically and found to have an effect on the buffet pressure response on the rigid vertical tails. Measured pressure time histories and power spectral densities were evaluated for each transducer for 35 configurations. The results show the parabolic fillet shape to cause the most amount of tail buffet pressure response. A diamond fillet shape caused the least amount of tail buffet response and had less buffet pressure response then the condition of no fillet at the wing/strake juncture. Also, the diamond fillet caused a frequency shift compared to the baseline configuration that may be important for buffet alleviation. Buffet pressure response was seen to vary with angle-of-attack. Buffet frequency depended on transducer location on the vertical tail as well as fillet shape, spanwise tail location, and angle-of-attack. A low frequency pulse (less than 1 Hz) was found to have a tremendous amount of energy. At present, this pulse is believed to be the result of the movement of the vortex breakdown location.

ACKNOWLEDGEMENTS

The research was supported by the Office of Naval Research. Mr. Bill King was the program manager. Computer resources provided by Department of Defense High Performance Computer facilities located at Army Research Laboratory, Aberdeen, MD.

REFERENCES

1. Washburn, A.E., Jenkins, L.N., and Ferman, M.A., "Experimental Investigation of Vortex-Fin Interaction," AIAA 31st Aerospace Sciences Meeting and Exhibit, AIAA 93-0050, Reno, NV, January 1993.

2. HTP-5 Workshop on Vortical Flow Breakdown and Structural Interactions. NASA Langley Research Center, Hampton VA, August 1991.

3. Kandil, O.A., Sheta, E.F., and Massey, S.J., "Twin Tail/Delta Wing Configuration Buffet due to Unsteady Vortex Breakdown Flow," *Proceedings of the 14th AIAA Applied Aerodynamics Conference*, AIAA 96-2517-CP, New Orleans, LA, June 1996.

4. Findlay, D., "Numerical Analysis of Vertical Tail Buffet," AIAA 35th Aerospace Sciences Meeting and Exhibit, AIAA 97-0621, Reno, NV, January 1997.

5. Kern, S.B., "Vortex Flow Control Using Fillets on a Double-Delta Wing," *AIAA Journal of Aircraft*, Vol. 30, No. 6, November-December 1993.

6. Kern, S.B., "Investigation of Vortex Flow Control Using Fillets at the Strake/Wing Junction of a Double-Delta Wing," M.S. Thesis, The Pennsylvania State University, May 1992.

7. Bendat, J.S., and Piersol, A.G., *Engineering Applications of Correlation and Spectral Analysis*, Wiley Publishing, 1980.

8. Welch, P.D., "The Use of Fast Fourier Transform for the Estimation of Power Spectra: A Method Based on Time Averaging Over Short, Modified Periodograms," *IEEE Trans. Audio Electroacoust.*, Vol. AU-15, June 1967.

9. Mabey, D.G., "Some Aspects of Aircraft Dynamic Loads Due to Flow Separation," AGARD-R-750.

10. Lamborne, N.C., and Bryer, D.W., "The Bursting of Leading Edge Vortices; Some Observations and Discussion of the Phenomenon," Aeronautical Research Council, R&M No. 3282, 1961.

11. Lowson, M.V., "Some Experiments with Vortex Breakdown," *Journal of the Royal Aeronautical Society*, Vol. 68, May 1964.

12. Harvey, J.K., "Some Observations of the Vortex Breakdown Phenomenon," *Journal of Fluid Mechanics*, Vol. 14, 1962.

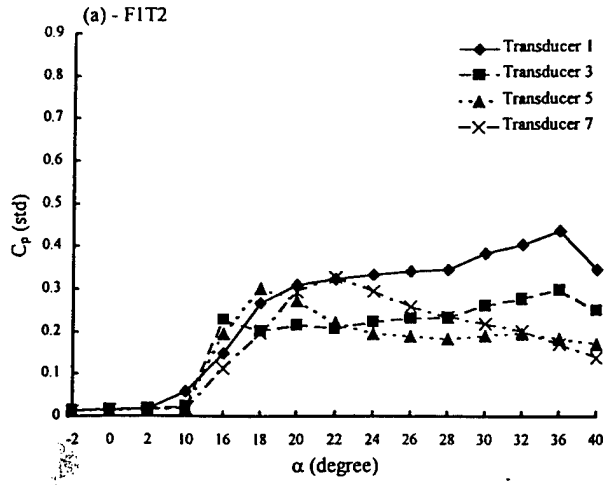

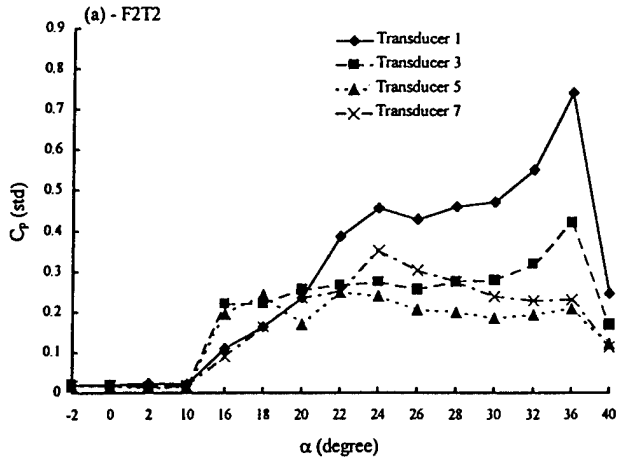

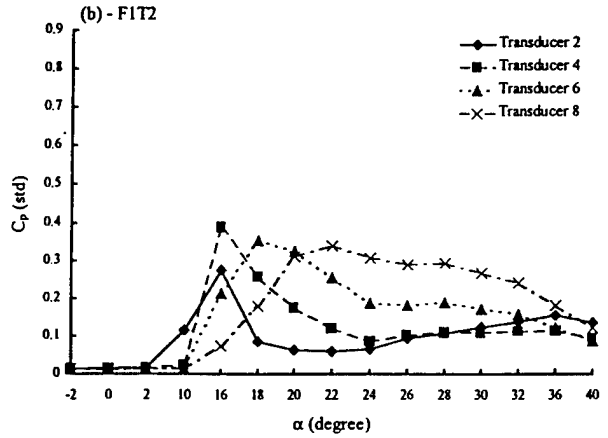

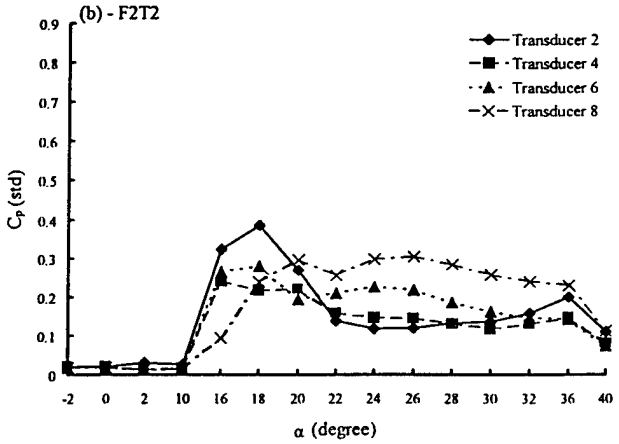

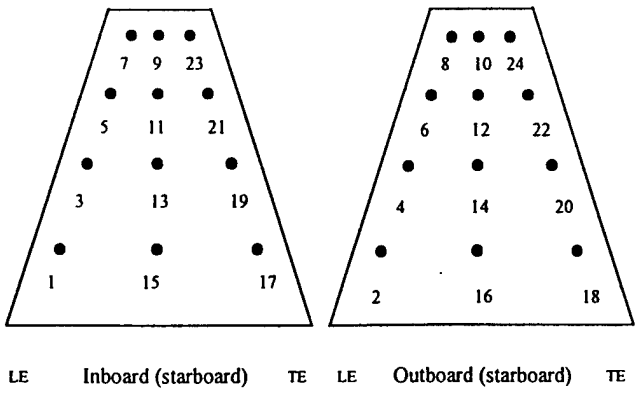

Figure 6 – C_p (standard deviation) vs. α, F1T2 (a) Transducers 1,3,5,7 (b) Transducers 2,4,6,8

Figure 7 – C_p (standard deviation) vs. α, F2T2 (a) Transducers 1,3,5,7 (b) Transducers 2,4,6,8

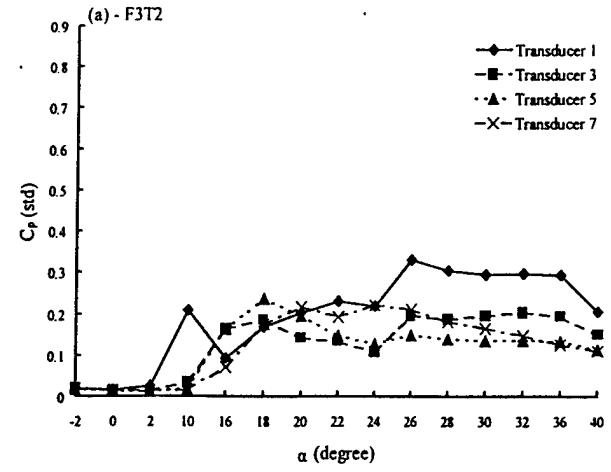

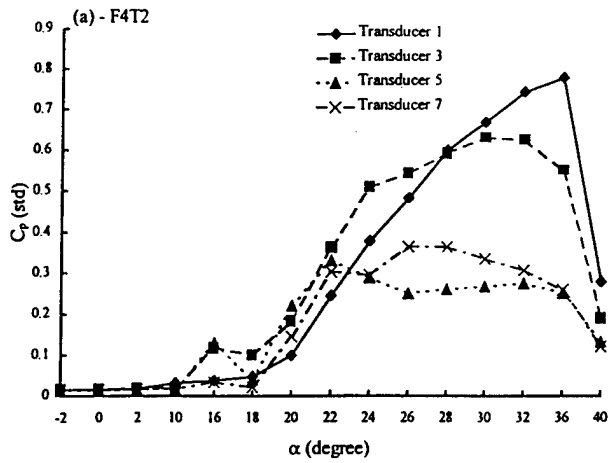

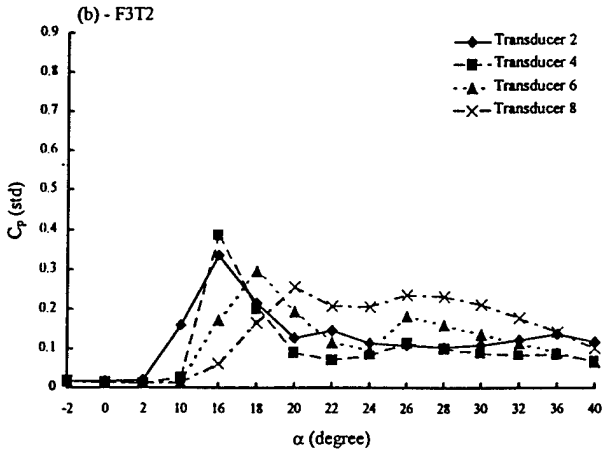

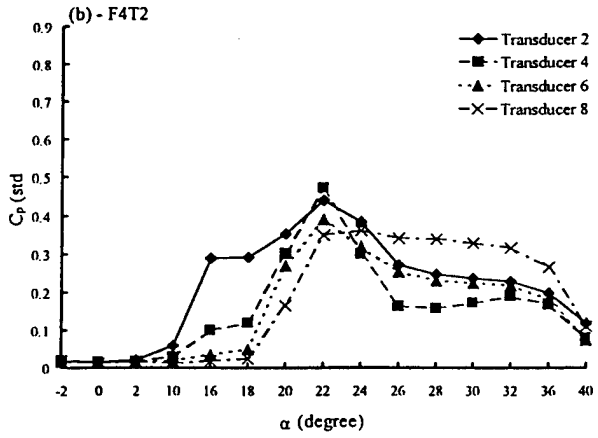

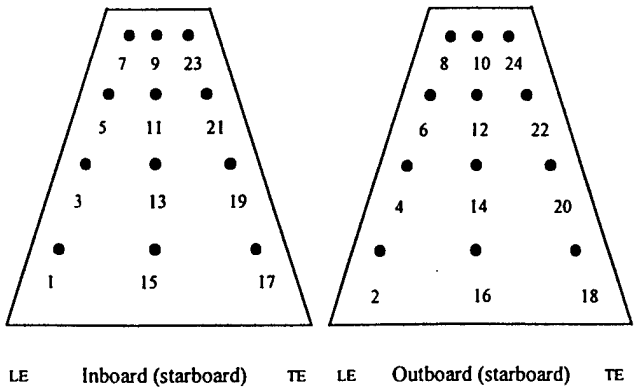

Figure 8 – C_p (standard deviation) vs. α, F3T2 (a) Transducers 1,3,5,7 (b) Transducers 2,4;6,8

Figure 9 – C_p (standard deviation) vs. α, F4T2 (a) Transducers 1,3,5,7 (b) Transducers 2,4,6,8

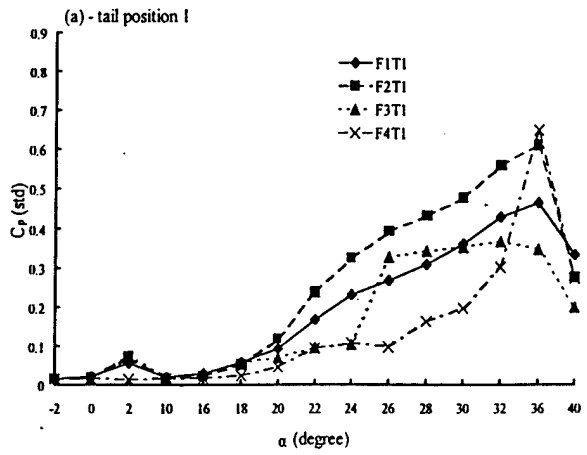

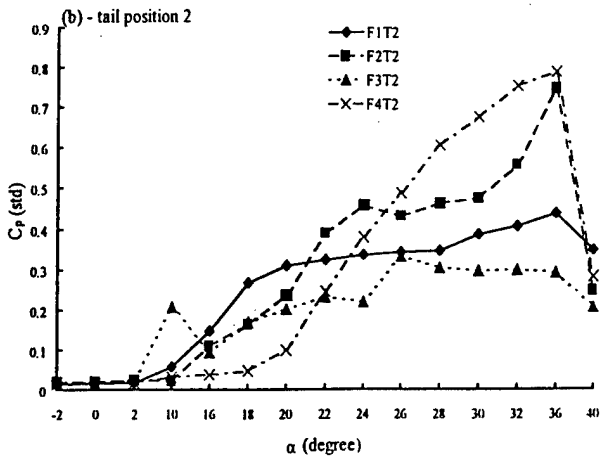

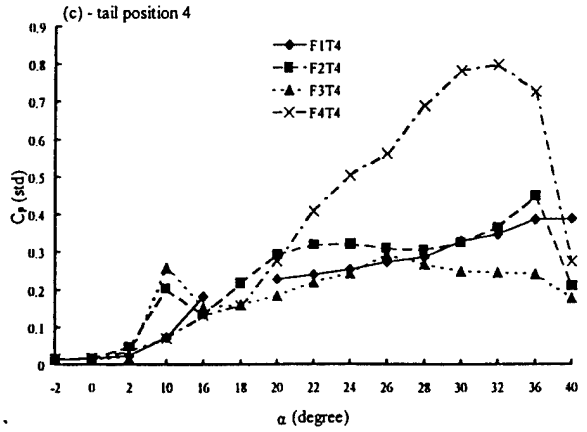

Figure 10 – C_p (standard deviation) vs. α, Transducer 1, (a) tail position 1, (b) tail position 2, (c) tail position 4

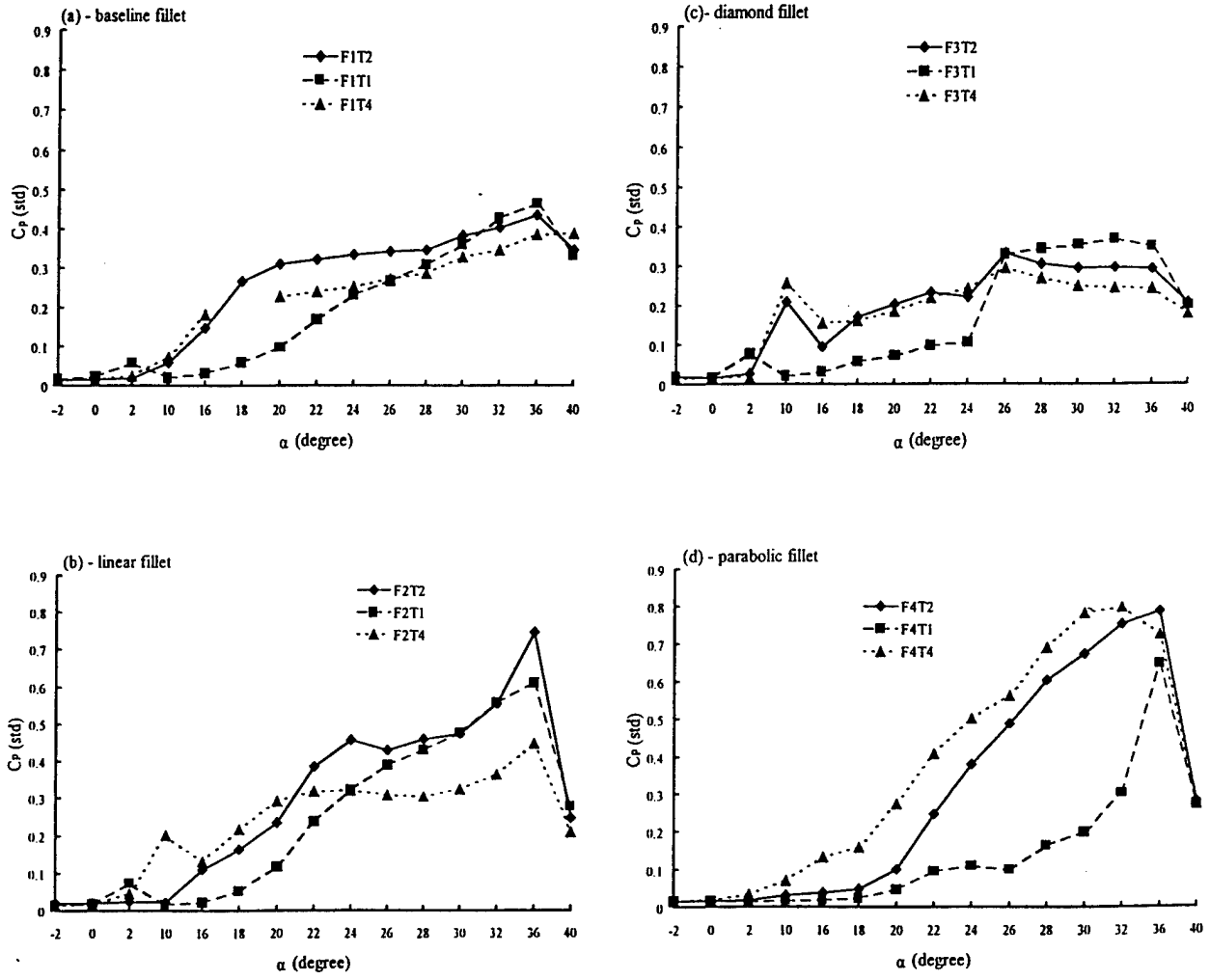

Figure 11 – C_p (standard deviation) vs. α, Transducer 1, (a) baseline fillet, (b) linear fillet, (c) diamond fillet, (d) parabolic fillet

F1T2			
St	Amplitude (St*PSD)$^{0.5}$	Transducer	α
1.1244	2.5731	1	30
1.0876	2.9825	1	32
1.0876	3.3041	1	36

F2T2			
St	Amplitude (St*PSD)$^{0.5}$	Transducer	α
1.6590	4.9708	1	32
1.5115	7.0468	1	36

F3T2			
St	Amplitude (St*PSD)$^{0.5}$	Transducer	α
1.8433	3.2164	4	16
1.7512	2.1345	1	30
1.7512	2.2807	1	32

F4T2			
St	Amplitude (St*PSD)$^{0.5}$	Transducer	α
1.8986	7.3392	4	22
1.7143	9.1452(C)	3	30
1.7143	6.9006	1	32

F1T1			
St	Amplitude (St*PSD)$^{0.5}$	Transducer	α
1.5115	5.1170	6	22
1.4009	2.3099	1	30
1.3088	2.8363	3	32
1.2719	3.3918	3	36

F2T1			
St	Amplitude (St*PSD)$^{0.5}$	Transducer	α
2.3410	1.9006	3	22
2.5806	2.8070	3	24
1.5668	4.4444	1	32
1.3641	4.6199	3	36

F3T1			
St	Amplitude (St*PSD)$^{0.5}$	Transducer	α
1.6037	2.1637	3	30
1.6221	3.3041	1	32

F4T1			
St	Amplitude (St*PSD)$^{0.5}$	Transducer	α
1.4931	7.0468	6	30
1.3273	7.1930	8	32

F1T4			
St	Amplitude (St*PSD)$^{0.5}$	Transducer	α
1.6221	2.4561	7	24
1.1244	2.3977	1	32
1.0691	2.2515	1	36
1.2166	3.0944	1	40

F2T4			
St	Amplitude (St*PSD)$^{0.5}$	Transducer	α
1.4009	2.4854	1	32
1.3641	3.7427	1	36

F3T4			
St	Amplitude (St*PSD)$^{0.5}$	Transducer	α
1.5115	1.8713	8	20
1.6959	1.6959	1	32
1.4931	1.3743	1	36

F4T4			
St	Amplitude (St*PSD)$^{0.5}$	Transducer	α
1.7880	8.5673(C)	1	26
1.2535	7.6023(C)	1	32
1.2535	7.1053	1	36

Table 1 – Maximum amplitude with corresponding frequency

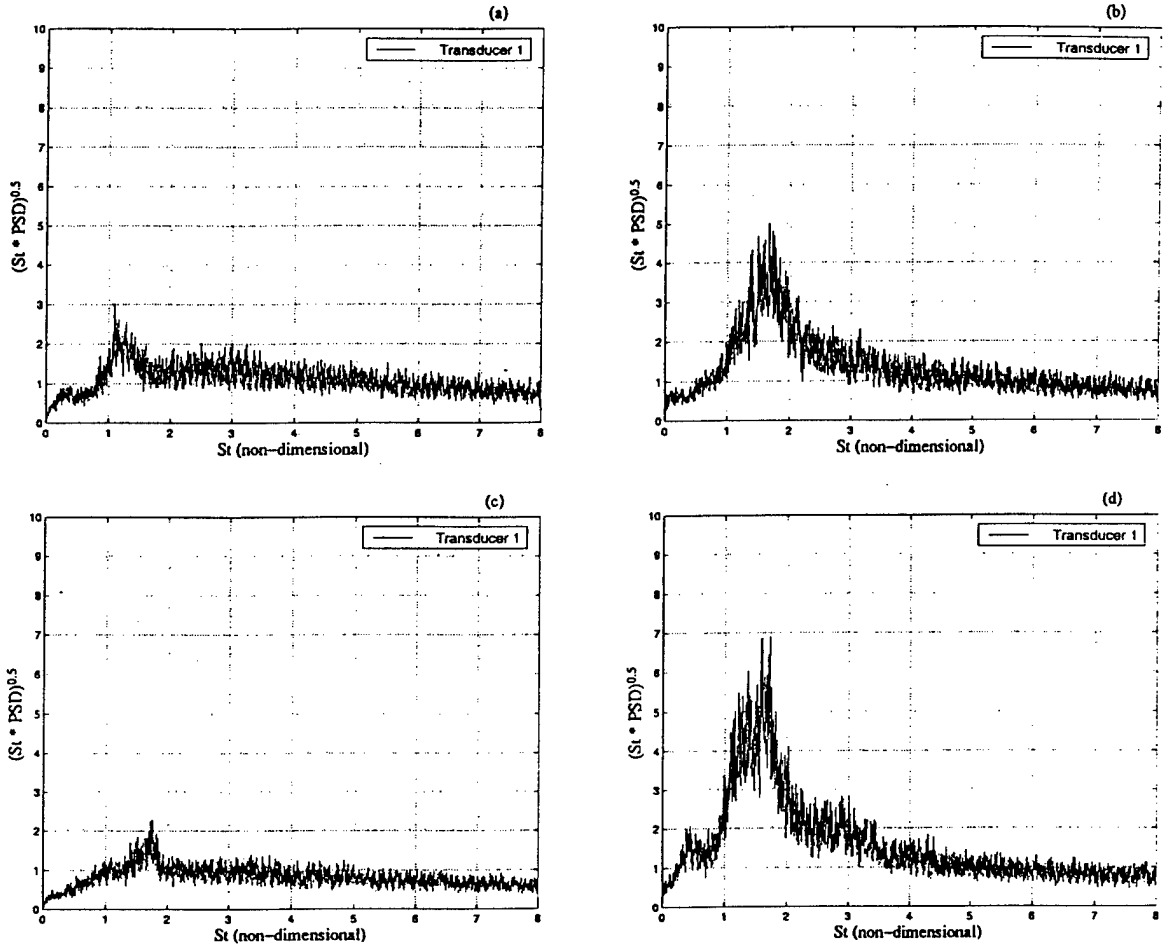

Figure 12- $(St*PSD)^{0.5}$ vs. Frequency: Transducer 1, $\alpha=32^{\circ}$, (a) F1T2 (baseline), (b) F2T2 (linear), (c) F3T2 (diamond), (d) F4T2 (parabolic)

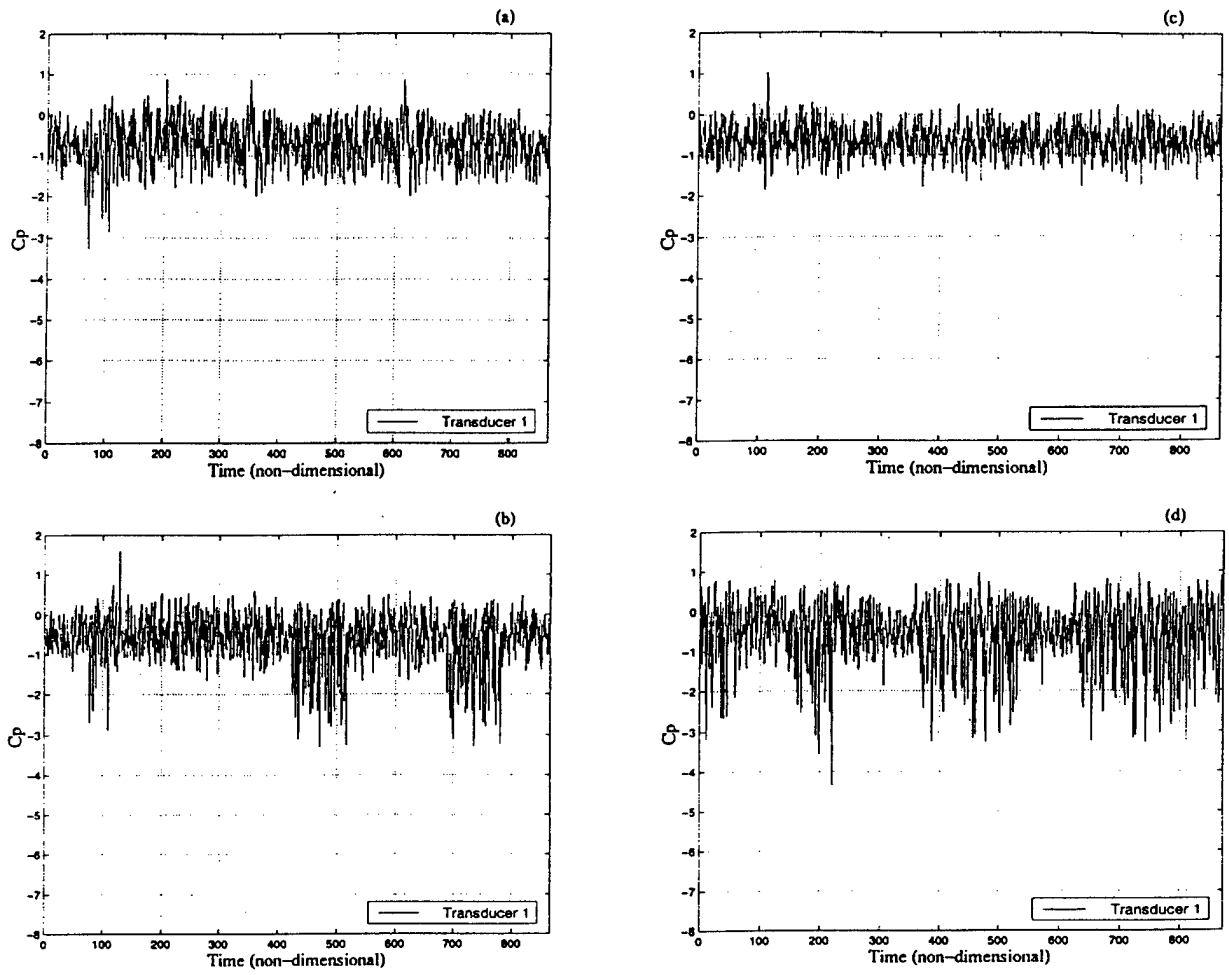

Figure 13- C_p vs. τ: Transducer 1, $\alpha=32^{\circ}$, (a) F1T2 (baseline), (b) F2T2 (linear), (c) F3T2 (diamond), (d) F4T2 (parabolic)

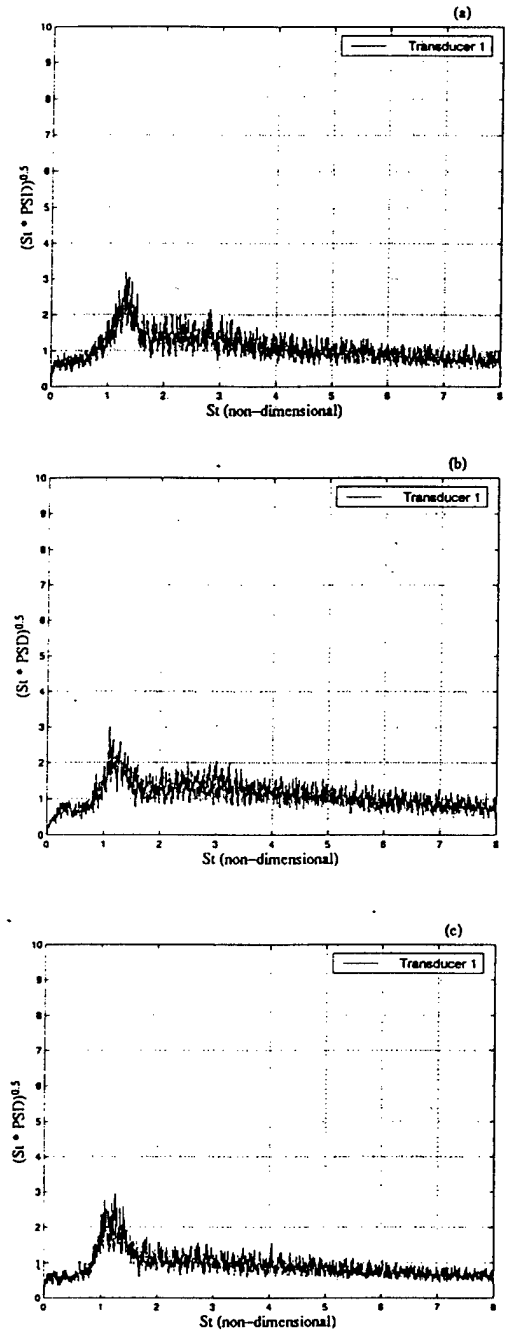

Figure 14- $(St*PSD)^{0.5}$ vs. Frequency: Transducer 1, $\alpha=32^{\circ}$, varying tail position, baseline (a) F1T1, (b) F1T2, (c) F1T4

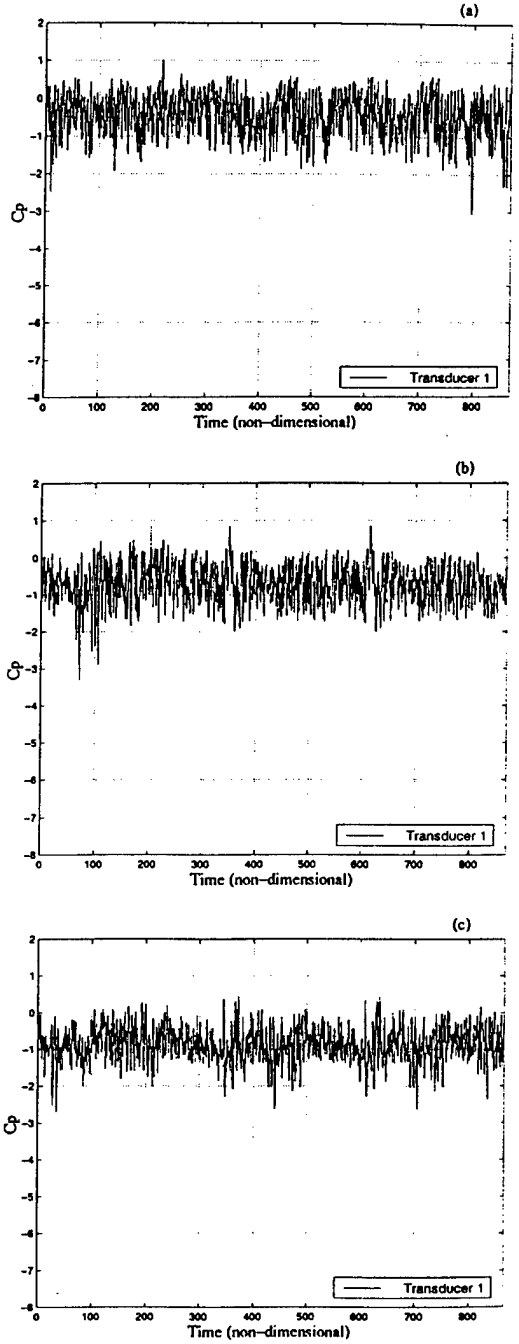

Figure 15- C_p vs. τ: Transducer 1, $\alpha=32^{\circ}$, varying tail position, baseline (a) F1T1, (b) F1T2, (c) F1T4

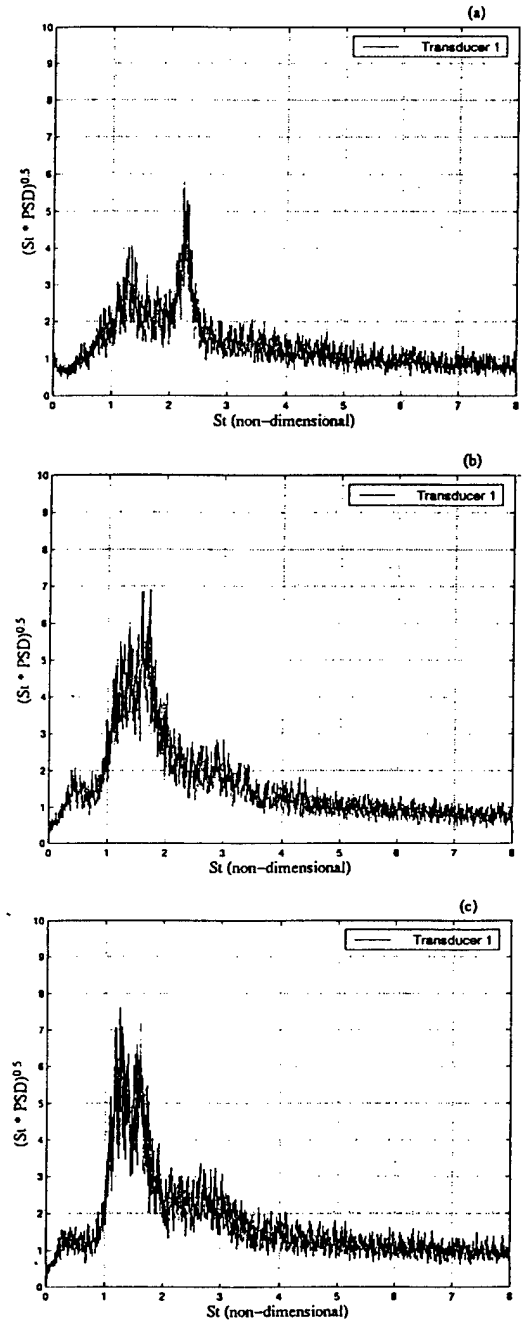

Figure 16- $(St*PSD)^{0.5}$ vs. Frequency: Transducer 1, $\alpha=32^{\circ}$, varying tail position, parabolic fillet (a) F4T1, (b) F4T2, (c) F4T4

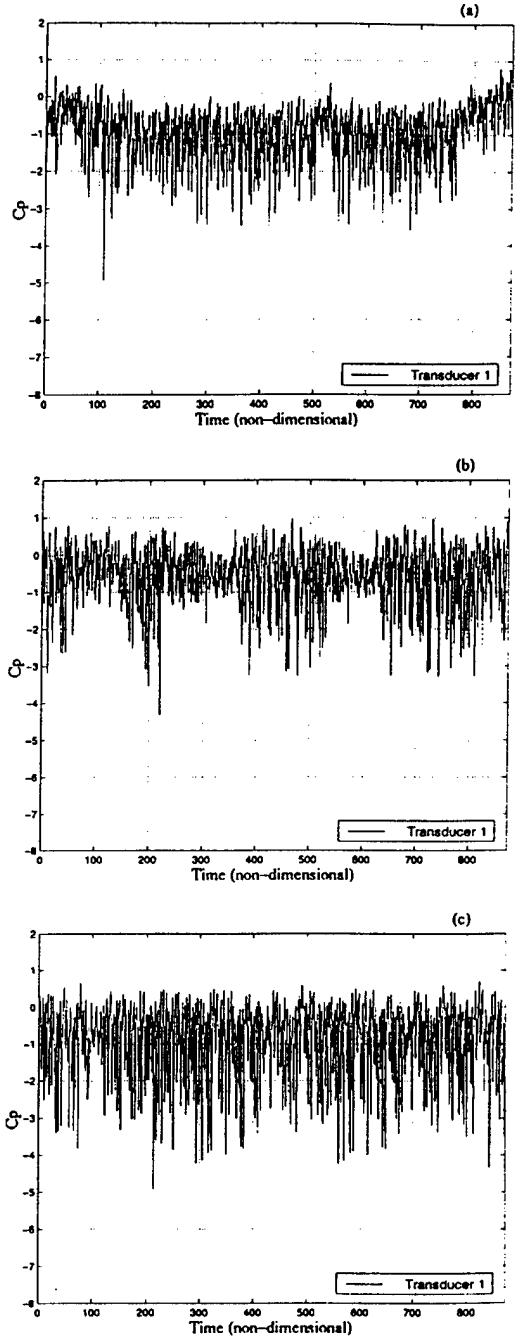

Figure 17- C_p vs. τ: Transducer 1, $\alpha=32^{\circ}$, varying tail position, parabolic fillet (a) F4T1, (b) F4T2, (c) F4T4

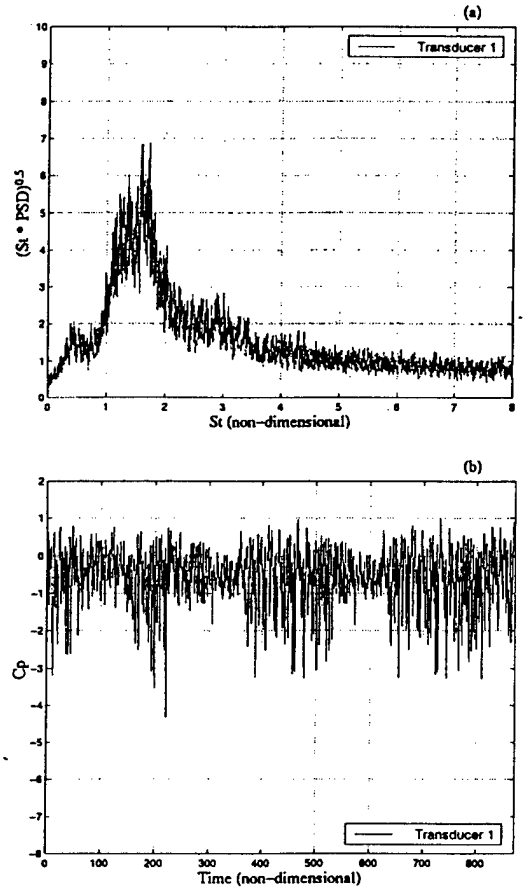

Figure 18- Transducer 1 (inboard), $\alpha=32^{\circ}$, F4T2 (a) $(St*PSD)^{0.5}$ vs. Frequency, (b) C_p vs. τ

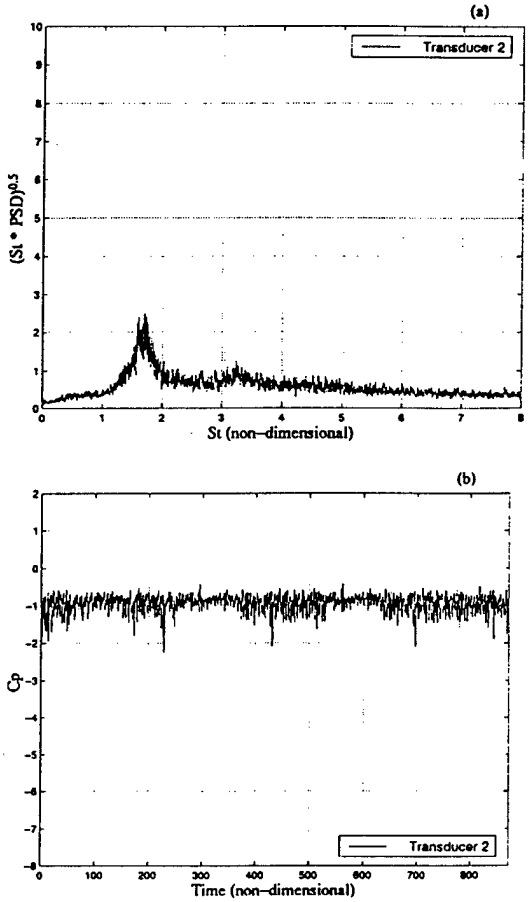

Figure 19- Transducer 2 (outboard), $\alpha=32^{\circ}$, F4T2 (a) $(St*PSD)^{0.5}$ vs. Frequency, (b) C_p vs. τ

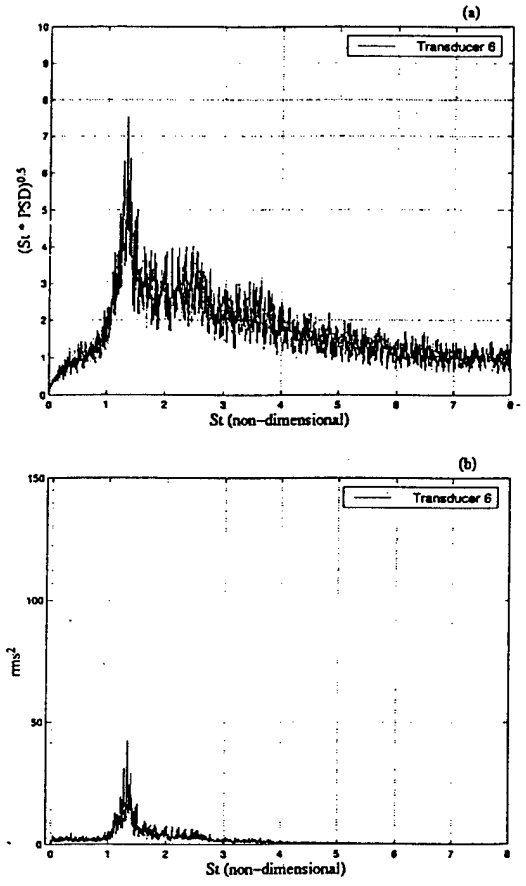

Figure 20- Power vs. Frequency, Transducer 6, $\alpha=32^{\circ}$, F4T1, (a) $(St*PSD)^{0.5}$ (b) PSD

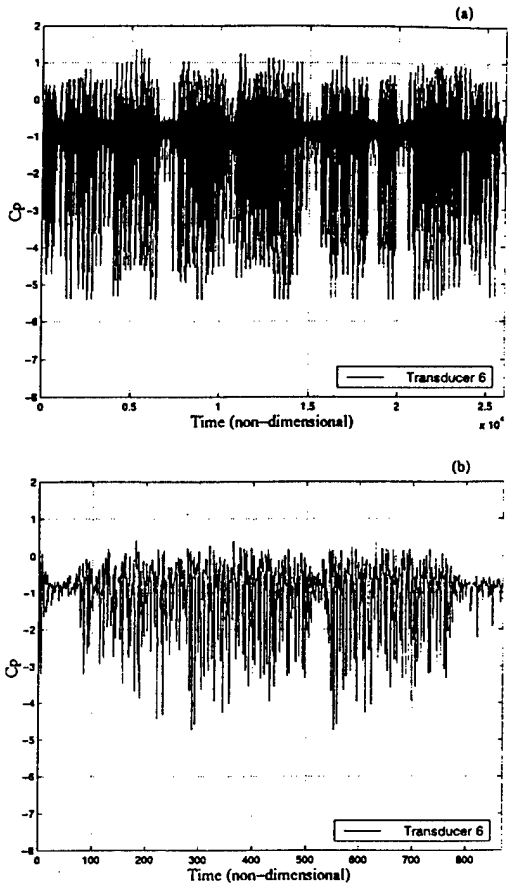

Figure 21- C_p vs. τ, Transducer 6, $\alpha=32^{\circ}$, F4T1, (a) 30 seconds, (b) 1 second

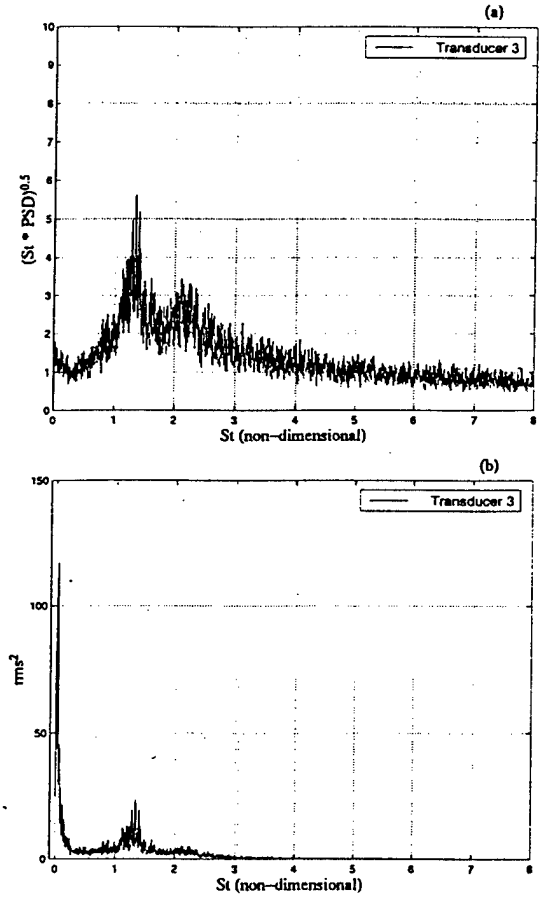

Figure 22- Power vs. Frequency, Transducer 3, $\alpha=32^{\circ}$, F4T1, (a) $(St*PSD)^{0.5}$ (b) PSD

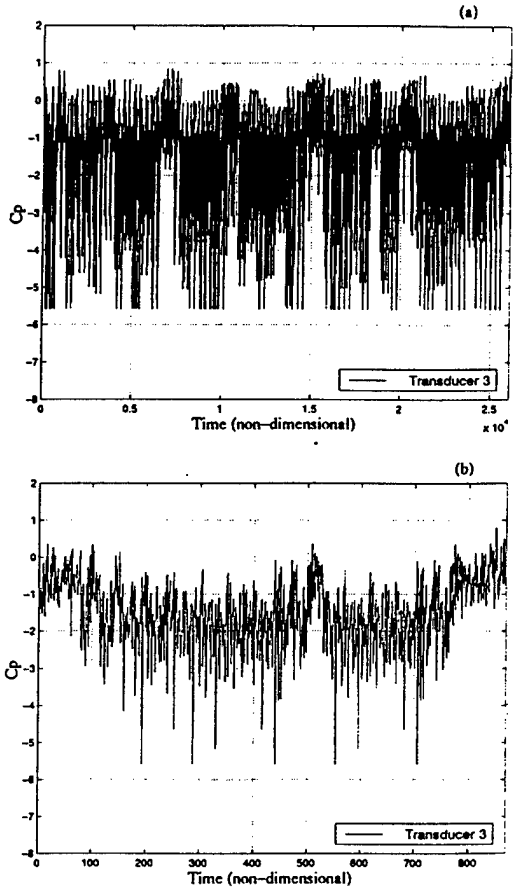

Figure 23- C_p vs. τ, Transducer 3, $\alpha=32^{\circ}$, F4T1, (a) 30 seconds, (b) 1 second